Proceedings of the Twentieth (2010) International Offshore and Polar Engineering Conference
Beijing, China, June 20–25, 2010

ISBN 978-1-880653-77-7 (Set); ISSN 1098-6189 (Set); www.isope.org

Coupling of NWT and Large-eddy Simulation for Wave-induced Sediment Transport

Jeffrey C. Harris and Stéphan T. Grilli
Department of Ocean Engineering, University of Rhode Island
Narragansett, RI, USA

ABSTRACT

We present the validation and application of a numerical model for the simulation of wave-induced sediment transport. Our approach is a one-way coupling of an inviscid flow model (i.e., a Numerical Wave Tank based on potential flow theory; NWT) to a Navier-Stokes solver, to simulate near bottom wave-induced turbulent boundary layer flows. Only two-dimensional incident wave fields have been considered so far (i.e., long-crested swells), while the near-field wave-induced turbulent flow and sediment transport are fully three-dimensional. Good results are obtained for steady streaming velocities when applying open boundary conditions (i.e., zero velocity gradient), a quarter-wavelength from the edge of the domain without the assumption of periodicity. For turbulent test cases, we solve the Navier-Stokes equations using a large-eddy simulation using an approximate (log-layer) wall boundary condition and a dynamic Smagorinsky subgrid scale model. After validating the model hydrodynamic predictions, we simulate wave-induced sediment transport over an idealized rippled bed, and find reasonable agreement with laboratory results for oscillatory flows over full-scale sand ripples. Both idealized and more realistic test cases are presented.

KEY WORDS: Computational Fluid Dynamics; Hybrid model coupling; Large eddy simulation; Wave-induced oscillatory flows; Steady streaming; Sediment transport; Sand ripples

INTRODUCTION

In this paper, we present the development and validation of a hybrid numerical model of wave-induced sediment suspension and transport in shallow water near (but outside) the surfzone. This study was initially motivated by the U. S. Navy's interest in mine burial prediction, which over 2000–2008 led to extensive experimental (e.g., Elmore et al., 2005; Guyonic et al., 2007) and some numerical (e.g., Hatton et al., 2007) studies on the subject. Similar research into the modeling seabed morphology was also motivated by interest in predicting scouring around submarine pipelines (e.g., Liang and Cheng, 2005). The present work is an improvement of earlier work by Gilbert et al. (2007), into sediment transport predicted by a Numerical Wave Tank (NWT).

In the absence of bottom obstacles, the velocity field of non-breaking water waves propagating over a smoothly varying seabed can be accurately represented by an irrotational flow core, with thin turbulent Boundary Layers (BLs) near the bottom and free surface. Moreover, for short distances of propagation (i.e., a few wavelengths), dissipation in these thin BLs does not significantly affect wave shape and kinematics. An object protruding from the seabed, however, creates a significant perturbation to the irrotational wave flow, in the form of shed vortices, extending over a a few significant diameters in each direction (see e.g., Grilli et al., 2003). Laboratory experiments in a wave tank with a mobile bed show that small changes in the bottom topography, as compared to the incident wavelength, usually only affect near-field flow velocities within 2–3 equivalent diameters of the object and thus have negligible effects on the propagation of incident surface waves (e.g., Voropayev et al., 1999). Using a full Navier-Stokes (NS) model to simulate a large part of the wave transformation region would both be prohibitive and also less accurate than using an irrotational model, as far as wave propagation is concerned, since NS schemes typically cause excessive numerical diffusion that damps incident waves in a non-physical manner. For this reason, hybrid models have already been introduced in earlier two-dimensional (2D) and three-dimensional (3D) work, which couple irrotational and Navier-Stokes (volume of fluid; VOF) models to study wave propagation and breaking, (e.g., Biausser et al., 2004).

In the proposed hybrid model, as in Gilbert et al. (2007), far-field incident waves and their transformations, over complex bottom topography from offshore to the obstacle, are simulated in an inviscid and irrotational 2D potential flow NWT, with fully nonlinear free surface boundary conditions (Grilli and Subramanya, 1996; Grilli et al., 2003). The 3D oscillatory BL flow induced by waves around the obstacle is then simulated in an embedded 3D large-eddy simulation (LES) of the turbulent fields similar to that of Zedler and Street (2006). The NWT approach allows simulation of 'far-field' wave transformations without the effect of the bottom obstacle, and thus provide background wave velocities for driving the 'near-field' 3D turbulent flow model around the bottom obstacle. Since observations indicate that a small obstacle does not significantly affect wave propagation over short distances, feedback from the 3D-NS model to the NWT can be neglected. Instead, the overall effect of bottom friction on wave shoaling is represented as a free surface dissipation

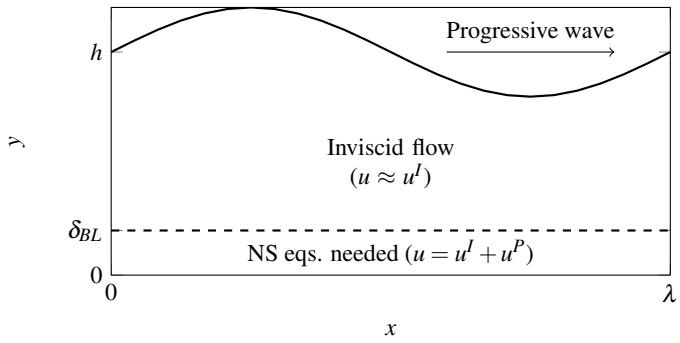

Fig. 1: Typical set-up of the embedded LES domain – the velocity u is decomposed into the inviscid velocity, u^I, and a perturbation, u^P, and the NS equations only need to be solved for the boundary layer (for $y < \delta_{BL}$).

in the NWT (see Grilli et al., 2003). Although it is more common to apply a Reynolds-averaged approach than a LES to solve NS equations, Chang and Scotti (2004) showed that a LES provides a better representation of flow over ripples, when considering the vertical velocity, turbulent kinetic energy, or Reynolds stresses.

Although the weakly coupled approach from Gilbert et al. (2007) appears sound, it is in a formalism that made it difficult to properly specify boundary conditions. Also, these earlier simulations did not extend over enough time to reach a quasi-periodic state, nor were they validated against experimental data. Finally, and perhaps more importantly, in the earlier model, waves effects were simply simulated in NS equations by the addition of an ad hoc wave-induced dynamic pressure gradient, whose theoretical justification was not fully rigorous. By contrast, in the present study, we decompose the total flow velocity and pressure into an irrotational wave flow and a viscous perturbation flow and solve NS equations for the perturbation flow only, using exact forcing terms calculated based on the irrotational wave flow. Note that many simple analytical/numerical solutions exist to obtain the latter, other than using a full NWT, which will be used both for theoretical and experimental validation. More advanced applications involving complex incident wave fields simulated in the NWT will be reported in future work. In the following, we present equations and boundary conditions for the hybrid model and its validation for some standard solutions of wave-induced flow and sediment transport in an oscillatory BL.

EQUATIONS FOR THE HYBRID MODEL

We briefly present equations for the one-way coupled hybrid model that is used here, whereby the irrotational wave flow in the NWT forces the LES computations, and resulting oscillatory turbulent BL, but the corresponding near-bottom dissipation does not affect the wave flow. The upper boundary between the LES domain and the rest of the NWT domain is determined *ad hoc*, and is roughly the height of the boundary layer, δ_{BL} (Fig. 1). Similar approaches have also been proposed by Kim et al. (2005) and Alessandrini (2007) who used Reynolds-averaged approaches to study ship waves. Note that in this hybrid approach, the inviscid velocity field is obtained directly from another model, and hence is not subject to the numerical errors of the NS solver.

Large-Eddy Simulation

The NS equations for an incompressible, isothermal, Newtonian fluid read:

$$\frac{\partial u_i}{\partial x_i} = 0; \qquad \frac{\partial u_i}{\partial t} + \frac{\partial}{\partial x_j}\left(u_i u_j + \frac{p}{\rho}\delta_{ij} - \nu\frac{\partial u_i}{\partial x_j}\right) = 0 \tag{1}$$

where u_i and p are the water velocity and dynamic pressure, respectively, in a fluid of density ρ and kinematic viscosity ν. We adopt the convention that x_2 is a vertical distance measured from a point on the seabed.

Many flows, such as those induced by ocean waves, can be closely represented by inviscid fields (u_i^I, p_I), which outside of thin BLs are described by Euler equations:

$$\frac{\partial u_i^I}{\partial x_i} = 0; \qquad \frac{\partial u_i^I}{\partial t} + \frac{\partial}{\partial x_j}\left(u_i^I u_j^I + \frac{p_I}{\rho}\delta_{ij}\right) = 0. \tag{2}$$

We introduce a decomposition of the total flow into an inviscid free-stream flow, with velocity u_i^I and pressure p_I, and a defect or perturbation flow, with velocity u_i^P and pressure p_P:

$$u_i = u_i^I + u_i^P; \qquad p = p_I + p_P. \tag{3}$$

Subtracting Eqs. 2 from Eqs. 1, yields governing equations for the perturbation fields as:

$$\frac{\partial u_i^P}{\partial x_i} = 0; \qquad \frac{\partial u_i^P}{\partial t} + \frac{\partial}{\partial x_j}\left(u_i u_j - u_i^I u_j^I + \frac{p_P}{\rho}\delta_{ij} - \nu\frac{\partial u_i}{\partial x_j}\right) = 0. \tag{4}$$

Applying a spatial-average operator (overbar) to the NS equations yields momentum equations for the resolved perturbation as:

$$\frac{\partial \bar{u}_i^P}{\partial x_i} = 0; \quad \frac{\partial \bar{u}_i^P}{\partial t} + \frac{\partial}{\partial x_j}\left(\bar{u}_i\bar{u}_j - \overline{u_i^I u_j^I} + \frac{\overline{p_P}}{\rho}\delta_{ij} - \nu\frac{\partial \bar{u}_i}{\partial x_j} + \tau_{ij}\right) = 0. \tag{5}$$

where $\tau_{ij} = \overline{u_i u_j} - \bar{u}_i\bar{u}_j$ is the subgrid scale (SGS) stress. Here we neglect the grid filtering of the inviscid velocities (i.e., assuming $\overline{u_i^I u_j^I} \approx u_i^I u_j^I$), since typically the LES grid has a much smaller scale than variations in the inviscid field. Note that, typically, SGS models only consider $\tau_{ij} - \tau_{kk}/3$, because the resolved turbulent pressure, $\bar{p}^*$, is different from the resolved hydrodynamic pressure: $\bar{p}^*/\rho = \bar{p}/\rho + \tau_{kk}/3$.

For turbulent applications, SGS stresses are expressed as:

$$\tau_{ij} - \frac{\delta_{ij}}{3}\tau_{kk} = -2\nu_T\bar{S}_{ij} \tag{6}$$

where ν_T is eddy viscosity and $\bar{S}_{ij}$ is resolved shear strain rate. The eddy viscosity is determined using the dynamic Smagorinsky model of Germano et al. (1991). Additionally, following Chow et al. (2005), the eddy viscosity is increased at the wall, in the SGS model, in order to augment the near-wall shear stresses. Specifically, following Zedler and Street (2006), for all points between the bed and a height $2\Delta x_1$, eddy viscosity is specified as:

$$(\nu_T)_{total} = (\nu_T)_{SGS} + \kappa u_* x_2 \cos^2\left(\frac{\pi x_2}{4\Delta x_1}\right). \tag{7}$$

This scheme increases the near-wall stress and smoothly varies the eddy viscosity from that in the inner wall modeled region to the outer region in the LES domain.

The governing equations are discretized as in Cui and Street (2001), i.e., using a finite-volume formulation with 2nd-order accuracy in both time and space on a non-staggered grid. The Quadratic Upstream Interpolation for Convective Kinematics (QUICK) (Leonard, 1979) scheme is used to discretize the convective terms of the fluid flow, and 2nd-order centered differences are used for the remaining terms. The convective terms are time integrated using the 2nd-order Adams-Bashforth technique, and the diffusive terms with a 2nd-order implicit Crank-Nicolson scheme. The Poisson equation for the pressure field is solved with a multigrid technique.

Velocity Boundary Conditions

The bottom boundary condition is a no-flux condition with a shear stress applied depending on the flow conditions, i.e., $\tau_w = \rho\nu\left[\partial u/\partial n\right]_{y=0}$, where τ_w is wall shear stress and n the normal direction to the wall. This is numerically implemented through ghost cells outside of the domain. Combining this with the condition that the eddy viscosity is zero along the bed, we can implement the boundary condition through the viscous stress terms as $\left[\partial u/\partial n\right]_{y=0} = u_*^2/\nu$, where u_* is the friction velocity, which is related to the wall shear stress as: $\tau_w = \rho u_*^2$. We apply one of two different boundary conditions, depending on the application.

For laminar cases, we consider a no-slip condition, such that

$$u_* = \sqrt{\frac{\bar{u}\nu}{z}} \tag{8}$$

where here $\bar{u}$ refers to the magnitude of the tangential velocity at height z above the bottom boundary. This condition is applied based on the locally resolved velocity at the gridpoint adjacent to the boundary.

For rough turbulent cases, we assume that the von Karman-Prandtl equation describing a logarithmic sub-layer can be applied at the first gridpoint above the bed. For hydraulically rough conditions, this reads:

$$\frac{\bar{u}}{u_*} = \frac{1}{\kappa}\log\frac{z}{z_0} \tag{9}$$

where κ is the von Karman constant, taken to be 0.41, and z_0 is roughness length, which can be related to the Nikuradse roughness as: $k_s = 30z_0$. Note, there is still some debate regarding the accuracy of using a log-layer assumption (see e.g., Stoll and Porté-Agel, 2006), but it is common practice to apply this in LES models of atmospheric flows (Moeng, 1984). For a review of LES wall modeling see Piomelli and Balaras (2002). The use of the log-layer law for zero-pressure gradient BLs is supported by the experiments of Nakayama et al. (2004), but especially when flow separation is important, more complicated boundary conditions may be required (e.g., Loureiro et al., 2008).

Suspended Sediment Concentration

An advection-diffusion equation governs the Suspended Sediment Concentration (SSC), C, with settling velocity w_s, as in Gilbert (2006):

$$\frac{\partial C}{\partial t} + \frac{\partial}{\partial x_j}\left(u_j C - w_s\delta_{i2}C - \kappa\frac{\partial C}{\partial x_j}\right) = 0 \tag{10}$$

where $\kappa = \frac{\nu}{\sigma}$ is the diffusivity and σ the Schmidt number (assumed to be 1.0 in this manuscript). In the context of the LES model, Eq. 10 becomes the spatially averaged advection-diffusion equation:

$$\frac{\partial \bar{C}}{\partial t} + \frac{\partial}{\partial x_j}\left(\bar{u}_j\bar{C} - w_s\delta_{i2}\bar{C} - \frac{\nu}{\sigma}\frac{\partial \bar{C}}{\partial x_j} + \chi_j\right) = 0 \tag{11}$$

where

$$\chi_j = \overline{u_j C} - \bar{u}_j\bar{C} = -\kappa_T\frac{\partial \bar{C}}{\partial x_j}. \tag{12}$$

This formulation of the SSC equation assumes that the sand concentration is low enough to prevent strong particle-fluid and particle-particle interactions beyond a constant settling velocity; the upper limit of concentration at which this assumption can be applied before other effects need to be considered is discussed by Villaret and Davies (1995) and Elghobashi (1994).

The motion of the sediment at the seabed is governed by bedload transport, the settling of suspended sediment, and sediment pickup. These processes can be represented using nondimensional parameters including the density ratio, $s = \rho_s/\rho$, the Shields parameter, θ, and the particle parameter, D_*:

$$\theta = \frac{u_*^2}{(s-1)gd} = \frac{\tau}{(\rho_s-\rho)gd} \quad \text{and} \quad D_* = d_{50}\left[\frac{(s-1)g}{\nu^2}\right]^{1/3}. \tag{13}$$

The onset of sediment motion on the seabed is determined by comparing the Shields parameter to its critical value, θ_{cr}, which can be found using an empirical expression from van Rijn (1993). For the sand used for the simulations in this paper, $d_{50} = 0.44$ mm and the latter yields a critical Shields number of $\theta_{cr} = 0.0314$. [Note, the effect of bed slope is neglected in this expression.] Similarly, for this sand, the same work predicts a constant settling velocity of 5.32 cm/s.

Sediment re-suspension is modeled using the empirical relationships proposed by van Rijn (1984) for noncohesive sediments with grain sizes between 200 μm and 2000 μm. Sediment pickup, which occurs for a Shields parameter greater than the critical value, is given by applying van Rijn's formula in an instantaneous sense, as suggested by Nielsen (1992):

$$P = 0.00033\left(\frac{\theta-\theta_{cr}}{\theta_{cr}}\right)^{1.5}\frac{(s-1)^{0.6}g^{0.6}d^{0.8}}{\nu^{0.2}} \tag{14}$$

Alternate pickup functions are discussed by van Rijn (1993). The pickup function acts as a boundary condition for the SSC. Since the eddy diffusivity, like the eddy viscosity, tends to zero at the bed, the gradient of the SSC is given by $P = -\kappa\partial\bar{C}/\partial n$.

The suspended sediment transport equations are discretized as in Cui and Street (2001), like the momentum equations, i.e., using a finite-volume formulation with 2nd-order accuracy in both time and space on a non-staggered grid. The Simple High Accuracy Resolution Program (SHARP) (Leonard, 1988) scheme is used to discretize the convective terms, and 2nd-order centered differences are used for the remaining terms. Note the SSC is expressed as a dimensionless volume fraction.

APPLICATIONS

Initial applications of this velocity perturbation approach were aimed at validating the model for simple cases, such as turbulent BLs over flat beds (see Grilli et al., 2009), for oscillatory currents, with zero mass transport. A full account of these is given in Harris (2010) and one such case is presented in a following section.

In progressive waves, a small but significant wave-induced mass transport is generated in the BL, which flows in the direction of wave propagation. This steady streaming is an important aspect of coastal bottom BLs, which strongly affects sediment transport and must be correctly represented in the model. This is studied in a following section.

Finally, we present an application of the full model to predicting sediment suspension and transport over a complex seabed, represented by a ripple of idealized but realistic geometry.

Oscillatory turbulent BL

We simulate Jensen et al. (1989)'s laboratory experiment #13, for a horizontally uniform oscillatory flow in a flume (U-tube), defined as $u_i^I = \delta_{i1}U_0\sin\omega t$, with: $U_0 = 2.00$ m/s, $T = 9.72$ s ($\omega = 2\pi/T$), $\nu = 1.14\times10^{-6}$ m^2/s, and $k_s = 0.84$ mm. We then compute the mean velocity and Reynolds stresses, which were measured as a function of time and elevation over the rough bed in the BL.

To compare simulations and experiments, we average the relevant field variables over horizontal planes and at each half-period between $5T$ and $10T$. A fine grid with 128x32x64 cells is used, slightly larger than that used by Radhakrishnan and Piomelli (2008) who recently reported on

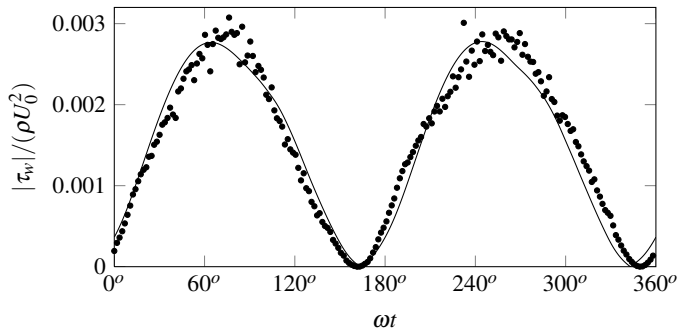

Fig. 2: Simulations of turbulent oscillatory BLs: mean wall stress as a function of phase (determined by log-law for test #13 of Jensen et al. (1989).

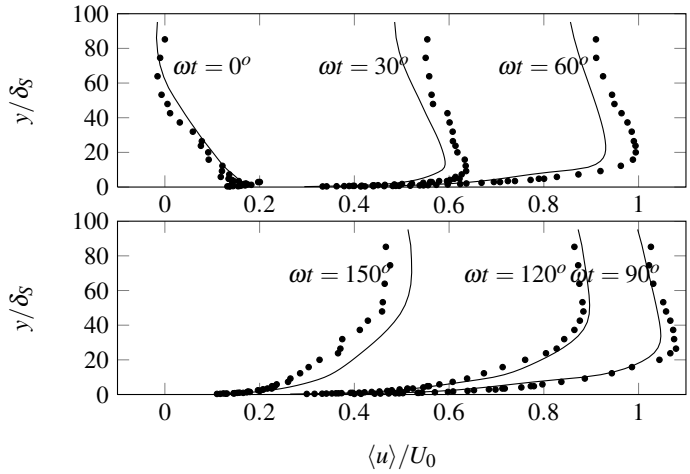

Fig. 3: Same as Fig. 2: mean streamwise velocity profiles for test #13 of Jensen et al. (1989).

similar comparisons. The use here of a three-dimensional grid is important for resolving the spanwise turbulent fluctuations. Exponential stretching is used in the vertical direction with a stretching ratio of 1.1.

For test #13, Jensen et al. did not measure wall stress $\langle \tau_w \rangle$, but rather a time-series of the mean streamwise velocity at a very small height over the wall, $y/A = 0.0006$ (equivalent to $y \simeq 1.86$ mm), which we used together with a log-law assumption to calculate the experimental wall stress. Results in Fig. 2 shows a good agreement of model results with the latter (and hence these results would also reasonably predict the Shields parameter used later). Results in Fig. 3, for the mean flow velocity $\langle u \rangle$ at six selected phases of the flow over half a period of oscillation, are similarly in reasonable agreement with experiments.

A more demanding model validation test is to compare turbulent intensities to those measured in experiments. In Fig. 4, for instance, we see a good overall agreement between model and experimental values of streamwise turbulent intensities $\langle u'^2 \rangle^{1/2}$, although simulations underpredict turbulent intensities measured near the wall. Similar discrepancies were found in Radhakrishnan and Piomelli (2008)'s recent LES study (using different SGS models), who also compared their results to Jensen's test case #13. Their results for the near-wall turbulent intensity were similar to ours for most phases of the oscillations.

In our own tests, the near-wall discrepancies are likely due to the grid aspect ratio near the wall. In a grid where $\Delta x = \Delta y = \Delta z$, the resolved perturbation velocity $\tilde{u}_i^P$ would, generally speaking, include fluctuations for all scales larger than the grid, and none smaller, as the implicit grid-scale filter would average over the smaller scale fluctuations. The vertical stretching of the grid near the wall results in "pancake"-like cells, where Δx and Δy is much larger than Δz. As a result, the implicit grid-scale filter averages over many turbulent eddies, and the resolved turbulent fluctuations are much smaller in magnitude [which incidentally is related to why the enhanced eddy viscosity from Eq. 7 is needed].

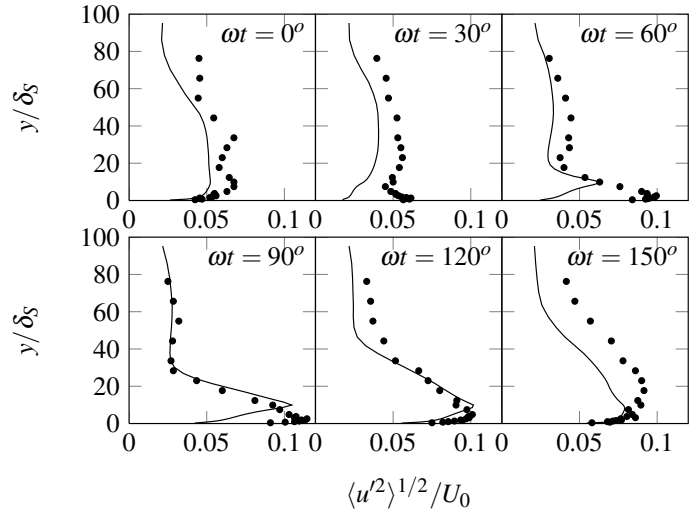

Fig. 4: Same as Fig. 2: streamwise turbulent intensity profiles for test #13 of Jensen et al. (1989).

Far from the wall, there is an occasional underprediction of the turbulent intensity. Other numerical studies have had this problem as well, which Mellor (2002) suggests is an experimental artifact. The amplitude of oscillations for test #13 is 3.1 m, so a fluid particle can move as far as 6.2 m over the course of each oscillation. Hence, at the end of each period (i.e., around 0^o), some of the fluid particles being measured may have been outside of the 10 m straight test section of the U-flume a half-period earlier. Although Jensen et al. took some additional measurements to attempt to show this would have no effect, it does seem to explain the outliers seen at the 0 degree phase angle (e.g., Fig. 4). Our results far from the wall are similar to Radhakrishnan and Piomelli's, although our turbulent intensities match experimental values somewhat better than theirs at phases 0^o and 30^o.

[Results similar to Fig. 4, not shown here, are obtained for the other Reynolds stress terms.]

Steady Streaming with Open Boundary Conditions

Longuet-Higgins (1953) was the first to show the occurrence of and calculate the mean mass transport velocity $\langle u \rangle$ induced in an oscillatory BL under progressive waves (i.e., steady streaming). This mean velocity occurs even when the forcing is from a fully symmetrical wave, such as obtained from linear wave theory, although flow asymmetries resulting from wave nonlinearity will intensify it, through the creation of a nonlinear Stokes drift. Thus, using linear wave theory for simplicity, the particle velocities in a progressive water wave over a flat bed are given by (see e.g., Dean and Dalrymple, 1991):

$$u_1^I(x,y,t) = A\frac{gk}{\omega}\frac{\cosh ky}{\cosh kh}\cos(kx-\omega t) \tag{15}$$

$$u_2^I(x,y,t) = A\frac{gk}{\omega}\frac{\sinh ky}{\cosh kh}\sin(kx-\omega t) \tag{16}$$

for an amplitude A, wavenumber k, and angular frequency ω. While this can be applied for any amplitude, this equation assumes a small wave

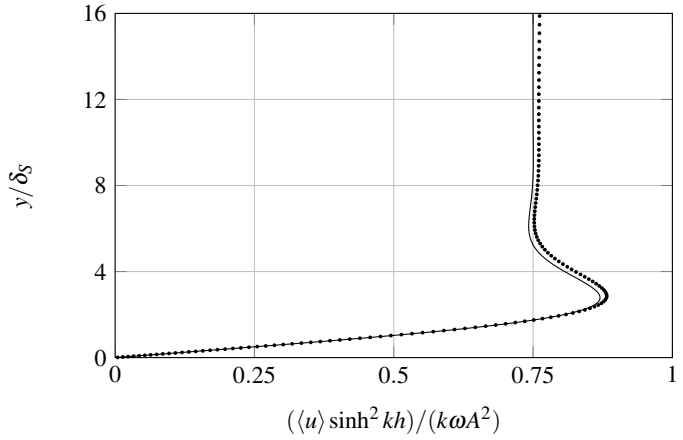

Fig. 5: Eulerian drift predicted by NS solver (·) versus theory (−).

steepness, $kH/2$. Additionally, the linear dispersion relation reads: $\omega^2 = k\tanh kh$, with h the water depth. For such waves, Longuet-Higgins found the Eulerian drift of a laminar oscillatory BL as:

$$\langle u\rangle = \frac{k\omega A^2}{\sinh^2 kh}\left[\frac{3}{4} - e^{-\xi}\cos\xi + \frac{1}{2}e^{-\xi}\sin\xi + \frac{1}{4}e^{-2\xi} - \frac{1}{2}\xi e^{-\xi}\cos\xi - \frac{1}{2}\xi e^{-\xi}\sin\xi\right] \tag{17}$$

where $\xi = z/\delta_S$ (Longuet-Higgins, 1958; Nielsen, 1992) and $\delta_S = \sqrt{2\nu/\omega}$ is the so-called Stokes-layer thickness.

In the model, assuming 2D periodic case, we specify periodic boundary conditions in the horizontal directions. The domain is uniformly discretized in the streamwise and vertical directions (and the spanwise direction is irrelevant for this 2D laminar case, in contrast to the turbulent case). No eddy viscosity was consider in this laminar case. Finally, rather than solving for the perturbation pressure to enforce mass conservation, we note that $u_2(x,z,t) << u_1(x,z,t)$ in this case, so that we can ignore the vertical momentum equation and instead compute the vertical velocity from mass conservation:

$$\tilde{u}_2^P(x_2) = -\int_0^{x_2} \frac{\partial \tilde{u}_1^P}{\partial x_1} dz' \tag{18}$$

This is an *ad hoc* solution, whereas a more appropriate solution would include a pressure boundary condition. [As pointed out by Mouazé et al. (2002), it is not clear what form an explicit boundary condition should look like in the far-field. Future work will focus on resolving this far-field boundary condition so that more accurate simulations can be conducted.] Because this bypasses the Poisson equation solver, which is normally used in the model to calculate pressure, the speed of computations with the NS solver is dramatically increased. However, using a correct pressure boundary condition would be more accurate and consistent. Preliminary tests suggest that setting the perturbation pressure to zero along the upper boundary gives good results and is consistent with the velocity boundary condition, but we have not applied it in these tests.

In this application, we compute steady streaming for periodic waves with $A = 0.23$ m and $T = 6$ s, in depth $h = 5$ m. [These are incidentally the conditions from an example used by Myrhaug and Holmedal, 2005.] We use a grid of 256 points in the streamwise and 32 points in the vertical directions, and a time step $\Delta t = T_0/256$. With this data, the spatial grid covers one wavelength ($2\pi/k$) in horizontal by $16\delta_S$ in vertical direction. Results in Fig. 5 show that the calculated Eulerian drift velocity, after a long ramp-up and model stabilization time of 1000 wave periods, agrees very well with theoretical Eq. 17.

The convergence of model results to the theoretical solution is assessed by calculating the difference between the steady streaming velocity highest point in the domain, u_∞, versus the theoretical solution, first as a function of discretization, and then boundary conditions.

In Fig. 6, we see an approximate 1st-order dependence of the solution on grid size in the vertical direction (from 16 to 128).

While the above results confirm that the model produces relevant results, applicable to wave-induced BLs, these were obtained from a spatially periodic solution in the lateral directions with a computational domain length L_x equal to one wavelength $\lambda = 2\pi/k$. In most practical applications, however, one needs to specify open boundary conditions (BCs) instead. In earlier work, (e.g., Gilbert et al., 2007) used BCs of the type: $\partial u/\partial n = 0$. Because of the need of correctly representing steady streaming in wave-induced BLs, it is important to investigate effects of such non-periodic BCs on simulated steady streaming velocities. In the present perturbation scheme, we thus specify $\partial u^P/\partial n = 0$ on lateral boundaries (i.e., zero perturbation velocity gradient) and test the effects of such open BCs on results of the above test case. To test model behavior over several spatial orders of magnitude, for $L_x > \lambda$ and $L_x < \lambda$, we vary the computational domain length with respect to the wavelength as, $L_x = \lambda, 2\lambda, ..., 2^4\lambda$ and $L_x = \lambda, \lambda/2, ..., \lambda/2^4$. In order to preserve Δx and not alter the discretization error, this has the effect of changing the number of gridpoints at the same time. Specifically, for the large domains, we use $\Delta x = \lambda/32$, and for the small domains, $\Delta x = \lambda/256$.

In Fig. 7, we see that applying simple open BCs we achieve similarly good results for steady streaming velocities, as in the periodic domain, a quarter-wavelength from the edge of the domain. The gradient-free boundary condition is thus reasonably successful, as long as the NS domain is at least a wavelength long in the main flow direction. Simulating steady streaming in smaller domains would most likely require more sophisticated BCs.

Sediment Transport over Ripples

In order to validate the proposed velocity perturbation method for sediment transport over complex bathymetry, we consider the Mr5b63 experiment of van der Werf et al. (2007), who tested bi-harmonic (vertically uniform) oscillatory flows over a moving sandy bed, with free stream (forcing) velocity given by:

$$u_\infty(t) = U_1\cos(\omega t - \gamma) + U_2\cos(2\omega t - 2\gamma) \tag{19}$$

The phase shift $\gamma = \arccos[(\sqrt{U_1^2 + 8U_2^2} - U_1)/(4U_2)]$ is used so that at a starting phase $\omega t = 0$ the forcing flow velocity is also zero. In experiments, the sand grain diameter was $d_{50} = 0.44$ mm and the oscillatory

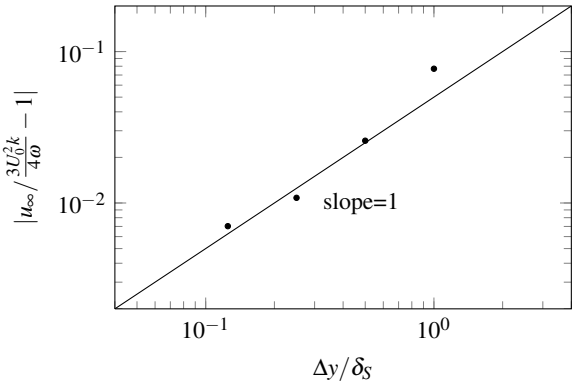

Fig. 6: Relative error in far-field Eulerian streaming velocity.

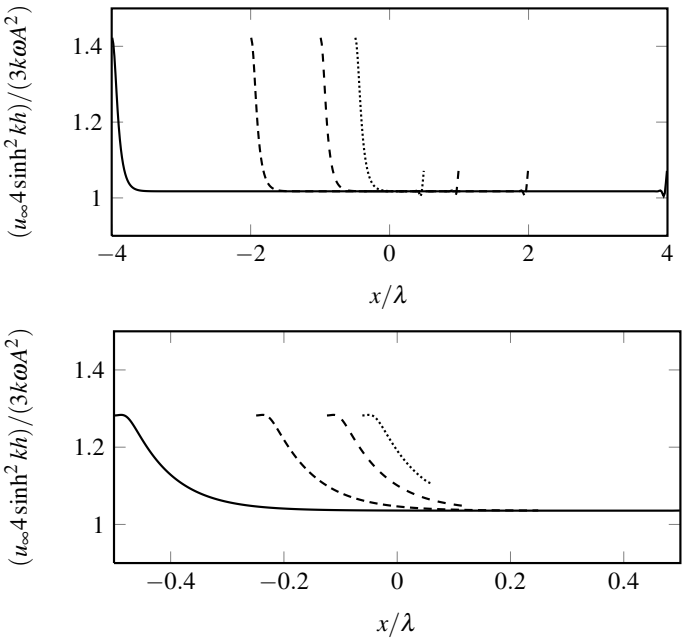

Fig. 7: Eulerian drift predicted by NS solver versus theory using open BCs for domains of length 8λ, 4λ, 2λ, and λ (upper) and λ, $\lambda/2$, $\lambda/4$, and $\lambda/8$ (lower).

flow had a period $T = 5.0$ s, with the first and second harmonics of the forcing velocity amplitude being $U_1 = 0.54$ and $U_2 = 0.095$ m/s, respectively. The test generated ripples with a wavelength of $2\pi/k = 0.41$ m, and a height of $\eta = 0.076$ m.

The LES had a domain of size $0.41 \times 0.35 \times 0.1$ m, discretized with a grid of $64 \times 64 \times 32$ points, with periodic boundary conditions in both the streamwise and spanwise directions. Here we model this case by considering flow over an idealized periodic ripple profile defined parametrically as:

$$x = \xi - \frac{\eta}{2}\sin k\xi \qquad \text{and} \qquad y = +\frac{\eta}{2}\cos k\xi. \tag{20}$$

which we then match to the dimensions of the experimentally generated ripples. The computational grid, over the (ξ,χ) domain, is given by the conformal mapping:

$$x = \xi - \frac{\eta}{2}\sin k\xi e^{-k\chi} \qquad \text{and} \qquad y = \chi + \frac{\eta}{2}\cos k\xi e^{-k\chi}. \tag{21}$$

A uniform grid spacing was used over the ξ direction and an exponential stretching was used over the χ direction (with a stretching ratio of 1.05). The governing equations were integrated in time over 10 periods of oscillation using a timestep of 0.5 ms (i.e., 100,000 timesteps). One can show analytically that combining Eq. 19 with Eqs. 21 results in the inviscid velocity:

$$u_1^I(\xi,\chi,t) = u_\infty(t)\frac{1 - \frac{1}{2}\eta k\cos(k\xi)\exp(-k\chi)}{1 - \eta k\cos(k\xi)\exp(-k\chi) + \frac{1}{4}\eta^2 k^2\exp(-2k\chi)} \tag{22}$$

$$u_2^I(\xi,\chi,t) = u_\infty(t)\frac{-\frac{1}{2}\eta k\sin(k\xi)\exp(-k\chi)}{1 - \eta k\cos(k\xi)\exp(-k\chi) + \frac{1}{4}\eta^2 k^2\exp(-2k\chi)}. \tag{23}$$

Ripple Shape. In Fig. 8, comparing the shape of the experimentally generated ripple profile with the analytic expression that we use for the LES domain, we see that the idealized ripple being used is steeper than the experimentally generated one. This could be corrected in future work by better matching the domains or numerically predicting the ripple profile (and inviscid flow), by taking into account a mobile seabed, but in our present investigation, we only consider a fixed seabed.

Velocity Field. In order to compare NS-LES results with experiment, we first process the particle image velocimetry (PIV) data of van der Werf et al. (2007), similarly to van der Werf et al. (2008). Specifically, the PIV data is a record of the sediment velocity, which is not necessarily the same as the fluid velocity, and no data was recorded in some gaps at the edges of the domain (e.g., from not having a high enough sediment concentration to obtain clear results). We corrected for these issues by horizontally applying a linear interpolation to the velocities at each height onto a 6.31 mm grid (i.e. 64 points per ripple wavelength). The velocity data was also assumed to be periodic, so that the gaps at the edges of the domain accordingly were filled in. Finally, the instantaneous horizontal average of the vertical velocity was removed at each height, corresponding to the application of mass conservation.

Fig. 9 shows an overall good agreement between velocity fields in NS-LES simulations and experimental results, at a phase angle of $\omega t = 120^o$ at which point a lee eddy or recirculation vortex exists. [Similar results (not shown) are found for all phases.] The biggest discrepancies may be due to the ripple shape – the sharper ripple crest in simulations results in a larger spawned eddy. The other likely reason is that the log-layer assumption used as a boundary condition is invalid when there are strong pressure gradients, which prominently occurs at the ripple crest.

Suspended Sediment Concentration. Fig. 10 shows there is several times more sediment suspension predicted by the LES than in experiments, but the general pattern and trends of the SSC field are rather similar. This could be due to a number of factors. In experiments, van der Werf et al. (2007) mentioned that the SSC was measured with an acoustic backscatter system (ABS), which may not have reported measurements very close to the bed where SSC would be higher but, first and foremost, that the ABS is only accurate to a factor of 2, which could account for much of the difference. In simulations, in addition to the different ripple shape, the LES ignored the effects that the SSC has on water density, which could be important particularly at the grid cells directly adjacent to the sand bed, where occasionally the SSC in small regions reaches values as high as 30% (which no-longer have negligible effects on fluid density). Although sediment is lifted from the vortex ripples in the eddies that are shed off of the ripple crests, the SSC near the bed could be much more similar than implied by Fig. 10.

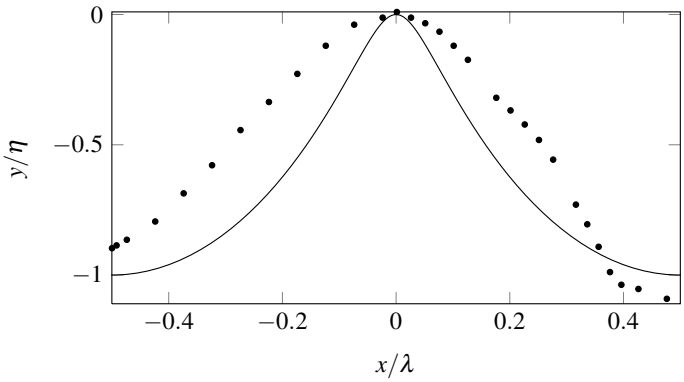

Fig. 8: Ripple shapes used for LES (–), and experimentally measured ripple profiles (·) from experiment Mr5b63 of van der Werf et al. (2007).

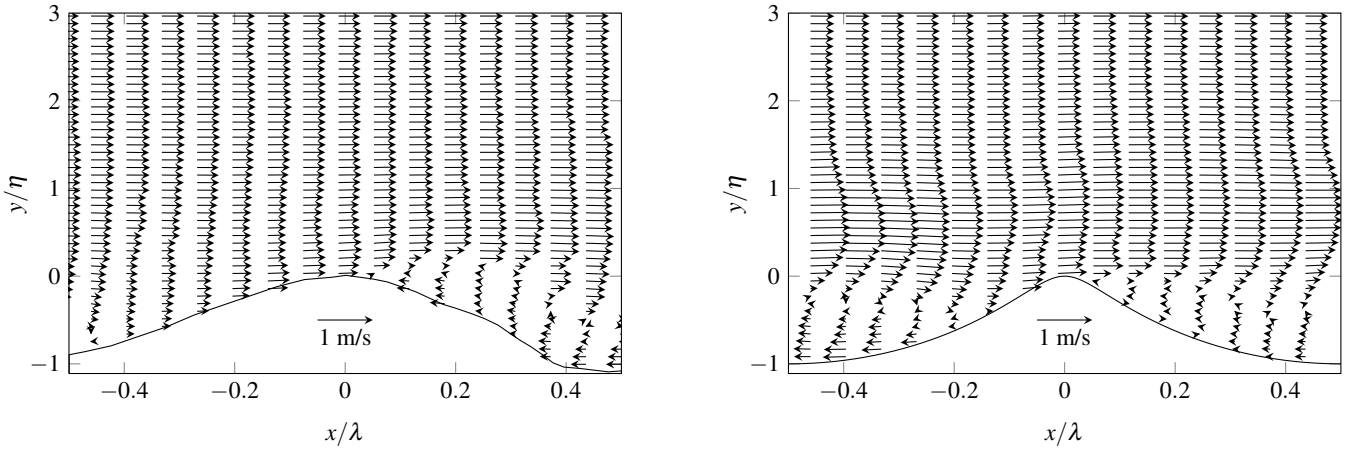

Fig. 9: Sample comparison of velocity field measured by experiment (left) and predicted by LES (right) at roughly $\omega t = 120^o$.

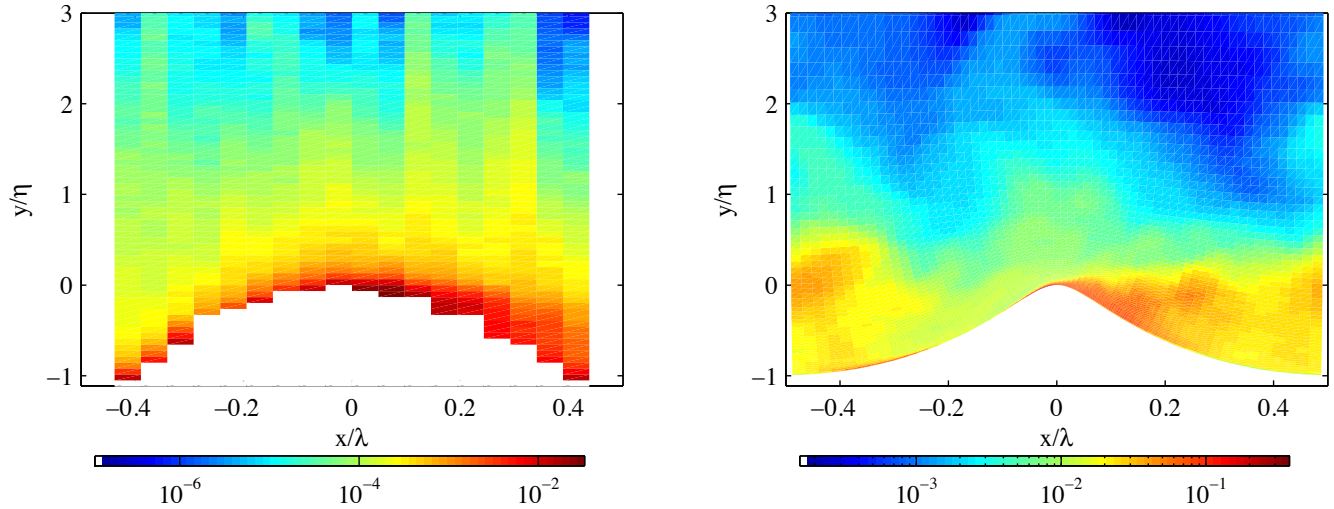

Fig. 10: Sample comparison of suspended sediment concentration (C) measured by experiment (left) and predicted by LES (right) at roughly $\omega t = 120^o$.

CONCLUSIONS

A perturbation approach to the Navier-Stokes (NS) equations, implemented using a Large-Eddy Simulation (LES), is validated for wave-induced BL flows and related sediment processes. This perturbation technique is likely to be particularly useful for coastal engineering problems, where the region of the seafloor requiring full NS modeling may be relatively small. Preliminary validation for turbulent oscillatory BLs was reported by (Grilli et al., 2009). Here, we considered this and additional cases of laminar steady streaming and oscillatory BLs over ripples.

We first showed the ability of the LES to predict the mean flow, wall stress, and second-order turbulent statistics for turbulent oscillatory BLs over a rough wall. All our results compared favorably with the experimental data of Jensen et al. (1989). Our simulations with dynamic SGS showed somewhat better agreement with the measured turbulent intensity far from the wall than the recent results of Radhakrishnan and Piomelli (2008). This may be due to using a gradient-free boundary condition, as opposed to setting the vertical velocity to zero in the free-stream, and to increased model accuracy when using the perturbation method.

We considered the two-dimensional case of a wave-induced BL. At first we limited our consideration to spatially-periodic boundary conditions in both lateral directions. Using linear wave theory to force the flow, we found that the computed steady streaming velocities in the BL closely matched those theoretically predicted by Longuet-Higgins (1958). By varying the number of vertical gridpoints, we further showed an approximate first-order convergence to the theoretical solution. We then considered the effect of open boundary conditions for non-periodic domains, by specifying $\partial u^P/\partial n = 0$ on lateral boundaries. This is one of the simplest open boundary conditions available and very similar to that used by Gilbert et al. (2007) in earlier work. We found that, in all cases considered, the steady streaming velocity agreed well with the theoretical solution, except with a quarter-wavelength from the open boundaries. This distance, over which the solution adjusts itself, was largest on the side of the domain where the waves were propagating from.

The LES was also shown to correctly reproduce some the major features of the flow over vortex ripples, including spawned lee eddies. We reprocessed data from van der Werf et al. (2007)'s experiments in order to validate the velocity and suspended sediment concentration fields. In particular, we considered a test case with vortex ripples were generated over a sandy bed, inside an oscillatory flow tunnel under rough turbulent conditions. Overall agreement was found to be reasonable, in view of the reported experimental errors. Note, our model results also compared favorably with the recent model results of van der Werf et al. (2008).

Future work may extend upon these results, in particular, by considering a seabed which moves over the course of the simulation in response to sediment pickup and bedload transport.

ACKNOWLEDGEMENTS

JH acknowledges support from an ONR-NDSEG fellowship. The project was supported in part by ONR Grant N000140510068 (MB program code 321CG). R. Street and O. Fringer are thanked for providing the initial LES code and J. van der Werf for experimental data.

REFERENCES

Alessandrini, B. (2007). *Thèse d'Habilitation en Vue de Diriger les Recherches*. PhD thesis, Ecole Centrale de Nantes.

Biausser, B., Grilli, S. T., Fraunie, P., and Marcer, R. (2004). Numerical analysis of the internal kinematics and dynamics of three-dimensional breaking waves on slopes. *Intl. J. Offshore and Polar Engng.*, 14(4):247–256.

Chang, Y. S. and Scotti, A. (2004). Modeling unsteady turbulent flows over ripples: Reynolds-averaged Navier-Stokes equations (RANS) versus large-eddy simulation (LES). *J. of Geophys. Res.*, 109(C09012).

Chow, F. K., Street, R. L., Xue, M., and Ferziger, J. H. (2005). Explicit filtering and reconstruction turbulence modeling for large-eddy simulation of neutral boundary layer flow. *J. of the Atmos. Sci.*, 62:2058–2077.

Cui, A. and Street, R. L. (2001). Large-eddy simulation of turbulent rotating convective flow development. *J. Fluid Mech.*, 447:53–84.

Dean, R. G. and Dalrymple, R. A. (1991). *Water wave mechanics for engineers and scientists*. World Scientific.

Elghobashi, S. (1994). On predicting particle-laden turbulent flows. *Appl. Sci. Res.*, 52:309–329.

Elmore, P. A., Richardson, M. D., and Friedrichs, C. T. (2005). Mine burial by scour in shallow seas: prediction and experiments. *Sea Tech.*, 46(3):10–15.

Germano, M., Piomelli, U., Moin, P., and Cabot, W. H. (1991). A dynamic subgrid-scale eddy viscosity model. *Physics of Fluids A*, 3(7):1760–1765.

Gilbert, R. W. (2006). Numerical modeling and validation of nonlinear wave driven sediment transport. Master's thesis, U. of Rhode Island.

Gilbert, R. W., Zedler, E. A., Grilli, S. T., and Street, R. L. (2007). Progress on nonlinear-wave-forced sediment transport simulation. *IEEE J. Oceanic Engng.*, 32(1):236–248.

Grilli, S. T., Harris, J. C., and Greene, N. (2009). Modeling of wave-induced sediment transport around obstacles. In *Proc. of the 31st Coastal Engng. Conf.*, pages 1638–1650, Hamburg, Germany.

Grilli, S. T. and Subramanya, R. (1996). Numerical modeling of wave breaking induced by fixed or moving boundaries. *Comp. Mech.*, 17:374–391.

Grilli, S. T., Voropayev, S., Testik, F. Y., and Fernando, H. J. S. (2003). Numerical modeling and experiments of wave shoaling over buried cylinders in sandy bottom. In *Proc. 13th Offshore and Polar Engng. Conf.*, pages 405–412, Honolulu, Hawaii.

Guyonic, S., Mory, M., Wever, T. F., Ardhuin, F., and Garlan, T. (2007). Full-scale mine burial experiments in wave and current environments and comparisons with models. *IEEE J. Oceanic Engng.*, 32(1).

Harris, J. C. (2010). *Wave-induced sediment transport: simulation of turbulent wave boundary layers*. PhD thesis, U. of Rhode Island.

Hatton, K. A., Foster, D. L., Traykovski, P., and Smith, H. D. (2007). Numerical simulations of the flow and sediment transport regimes surrounding a short cylinder. *IEEE J. Oceanic Engng.*, 32(1):249–259.

Jensen, B. L., Sumer, B. M., and Fredsoe, J. (1989). Turbulent oscillatory boundary layers at high Reynolds numbers. *J. Fluid Mech.*, 206:265–297.

Kim, K., Sirviente, A. I., and Beck, R. F. (2005). The complimentary RANS equations for the simulation of viscous flows. *Intl. J. Num. Meth. in Fluids*, 48:199–229.

Leonard, B. P. (1979). A stable and accurate convective modeling procedure based on quadratic upstream interpolation. *Comp. Meth. Appl. Mech. and Engng.*, 19:59–98.

Leonard, B. P. (1988). Third-order multi-dimensional Euler/Navier-Stokes solver. In *AIAA/ASME/SIAM/APS First National Fluid Dynamics Congress*, pages 226–231.

Liang, D. and Cheng, L. (2005). Numerical model for wave-induced scour below a submarine pipeline. *J. Waterway, Port, Coastal, and Ocean Engng.*, 131:193–202.

Longuet-Higgins, M. S. (1953). Mass transport in water waves. *Phil. Trans. of the Roy. Soc. of London A*, pages 535–581.

Longuet-Higgins, M. S. (1958). The mechanics of the boundary layer near the bottom in a progressive wave. In *Proc. 6th Intl. Conf. on Coastal Engng.*, pages 184–193.

Loureiro, J. B. R., Monteiro, A. S., Pinho, F. T., and Freire, A. P. S. (2008). The effect of roughness on separating flow over two-dimensional hills. *Experiments in Fluids*.

Mellor, G. (2002). Oscillatory bottom boundary layers. *J. of Phys. Oceanography*, 32(11):3075–3088.

Moeng, C.-H. (1984). A large-eddy simulation model for the study of planetary boundary-layer turbulence. *J. Atmos. Sci.*, 46:2311–2330.

Mouazé, D., Ourmières, Y., and Chaplin, J. R. (2002). Steady and unsteady flow in wave-induced boundary layers. In *Proceedings of the 17th International Workshop on Water Waves and Floating Bodies*.

Myrhaug, D. and Holmedal, L. E. (2005). Bottom friction caused by boundary layer streaming beneath random waves for laminar and smooth turbulent flow. *Ocean Engineering*, 32(2):195–222.

Nakayama, A., Noda, H., and Maeda, K. (2004). Similarity of instantaneous and filtered velocity fields in the near wall region of zero-pressure gradient boundary layer. *Fluid Dyn. Res.*, 35:299–321.

Nielsen, P. (1992). *Coastal bottom boundary layers and sediment transport*. World Scientific.

Piomelli, U. and Balaras, E. (2002). Wall-layer models for large-eddy simulation. *Annual Rev. Fluid Mech.*, 34:349–374.

Radhakrishnan, S. and Piomelli, U. (2008). Large-eddy simulation of oscillating boundary layers: model comparison and validation. *J. Geophys. Res.*, 113(C02022).

Stoll, R. and Porté-Agel, F. (2006). Effect of roughness on surface boundary conditions for large-eddy simulations. *Boundary-layer Meteorol.*, 118:169–187.

van der Werf, J. J., Doucette, J. S., O'Donoghue, T., and Ribberink, J. S. (2007). Detailed measurements of velocities and suspended sand concentrations over full-scale ripples in regular oscillatory flow. *J. Geophys. Res.*, 112(F02012).

van der Werf, J. J., Magar, V., Malarkey, J., Guizien, K., and O'Donoghue, T. (2008). 2DV modelling of sediment transport processes over full-scale ripples in regular asymmetric oscillatory flow. *Cont. Shelf Res.*, 28:1040–1056.

van Rijn, L. C. (1984). Sediment transport, Part I: bed load transport. *J. Hydraulic Engng.*, 110(10):1431–1456.

van Rijn, L. C. (1993). *Principles of sediment transport in rivers, estuaries and coastal seas*. Aqua Pub., Amsterdam, The Netherlands.

Villaret, C. and Davies, A. G. (1995). Modeling sediment-turbulent flow interactions. *Appl. Mech. Rev.*, 48(9):601–609.

Voropayev, S. I., McEachern, G. B., Boyer, D. L., and Fernando, H. J. S. (1999). Dynamics of sand ripples and burial/scouring of cobbles in oscillatory flow. *Appl. Ocean Res.*, 21(5):249–261.

Zedler, E. A. and Street, R. L. (2006). Large-eddy simulation of sediment transport: currents over ripples. *J. Hydraulic Engng.*, 132(2):180–193.